Rheology of concentrated suspensions of non-colloidal rigid fibres

Franco Tapia, Saif Shaikh, Jason E Butler, Olivier Pouliquen, Elisabeth Guazzelli

Rheology of concentrated suspensions of non-colloidal rigid fibres

Franco Tapia[1], Saif Shaikh[1,2], Jason E. Butler[2], Olivier Pouliquen[1] & Élisabeth Guazzelli[1]

[1]Aix Marseille Univ, CNRS, IUSTI, Marseille, France

[2]Department of Chemical Engineering, University of Florida, Gainesville, Florida 32611, USA

(Received xx; revised xx; accepted xx)

Pressure and volume-imposed rheology is used to study suspensions of non-colloidal, rigid fibres in the concentrated regime for aspect ratios ranging from 3 to 15. The suspensions exhibit yield-stresses. Subtracting these apparent yield-stresses reveals a viscous scaling for both the shear and normal stresses. The variation in aspect ratio does not affect the friction coefficient (ratio of shear and normal stresses), but increasing the aspect ratio lowers the maximum volume fraction at which the suspension flows. Constitutive laws are proposed for the viscosities and the friction coefficient close to the jamming transition.

1. Introduction

The rheological properties of viscous Newtonian fluids containing rigid fibres remains relatively unexplored as compared to suspensions of spherical particles, and a consensus on even the qualitative description of the rheology is still lacking for concentrations beyond the dilute limit. As one example, the steady values of the shear stresses should, for suspensions of fibres that are large relative to colloidal scales and free of external body forces, follow a Newtonian law (Dinh & Armstrong 1984). However, many experimental studies find yield stresses and a nonlinear scaling of the shear stresses with the rate of shear, where these non-Newtonian effects become more prominent with increasing concentration (Ganani & Powell 1985; Powell 1991). Different explanations have been proposed to explain the departure from a Newtonian response. This includes arguments that the fibres were not rigid under the imposed conditions (Powell 1991; Sepehr *et al.* 2004) or that the fibres are not force-free. An example of the latter is the assertion that adhesive forces (Mongruel & Cloitre 1999; Chaouche & Koch 2001; Bounoua *et al.* 2016*b*) can exist between the fibres, even though their size is large compared to typical colloidal scales.

Previous rheological studies have focused on suspensions at relatively small volume fractions. Identifying measurements of rheology for volume fractions, ϕ, above 0.1 is difficult for fibres of large aspect ratios, $A = L/d$, where L and d are the fibre length and diameter, respectively. The lack of data is attributable, at least in part, to the difficulty of preparing and measuring the rheology of suspensions at high concentrations for large aspect ratios. Even for aspect ratios as high as 17 or 18, measurements are available for volume fractions of only up to $\phi = 0.15$ or 0.17 (Bounoua *et al.* 2016*a*; Bibbó 1987); measurements as high as $\phi = 0.23$ were made by Bibbó (1987) for smaller aspect ratios of $A = 9$. As a result, the rheological properties of suspensions of rigid fibres remains to be characterised in the limit of large concentrations where mechanical contacts are expected to matter (Sundararajakumar & Koch 1997; Petrich & Koch 1998; Snook *et al.* 2014). Likewise, the volume fraction at which the shear stresses diverge, and the flow of the suspension ceases (i.e. becomes jammed), has not been determined previously

Fibre label	Symbol	A	L (mm)	d (mm)	S_p
(I)	□	14.5 ± 0.8	5.8 ± 0.1	0.40 ± 0.01	$5 \cdot 10^{-3}$
(II)	△	6.3 ± 0.4	2.5 ± 0.1	0.40 ± 0.01	$2.4 \cdot 10^{-4}$
(III)	◊	7.2 ± 0.4	5.8 ± 0.2	0.81 ± 0.02	$3.9 \cdot 10^{-4}$
(IV)	◯	3.4 ± 0.3	2.8 ± 0.1	0.81 ± 0.03	$2.7 \cdot 10^{-5}$

Table 1: Properties of each batch of fibres. Data shown includes the mean value and standard deviation of the aspect ratio A, fibre length L, and fibre diameter d. Values of the dimensionless number S_p, characterising the relative strengths of the viscous and elastic forces, are also reported.

for non-colloidal fibres, though such measurements have been made for shear-thickening suspensions of colloidal fibres (Egres & Wagner 2005; Brown *et al.* 2011).

Here, a custom-built rheometer has been used to explore the shear stresses and normal forces in suspensions of non-colloidal, rigid fibres for concentrations exceeding $\phi = 0.23$. The rheometer (Boyer *et al.* 2011; Dagois-Bohy *et al.* 2015) measures the stresses in both a pressure and volume-imposed configuration. The measurements indicate the presence of yield stresses in the tested suspensions, but also a viscous scaling wherein the stress grows linearly with the rate of shear. The unique rheometer design facilitates the study of these highly concentrated suspensions, and the volume fractions at which the stresses diverge are measured. The scaling of the stresses near this jamming transition are found to differ substantially from that of a suspension of spheres. These measurements are reported in § 3, after presenting the experimental materials and techniques in § 2; conclusions are drawn in § 4.

2. Experiments

2.1. *Fibres and fluids*

Four batches of rod-like particles were used in the experiments. They were obtained by using a specially-designed device to cut long cylindrical filaments of plastic (PLASTINYL 6.6) that were supplied by PLASTICFIBRE S.P.A. (http://www.plasticfibre.com). Images of typical fibres from each batch are shown in figure 1 (b). The length and diameter of over 100 fibres were measured with a digital imaging system. The distributions of lengths and diameters were found to be approximately Gaussian for all aspect ratios. The mean value and standard deviation of the fibre aspect ratio $A = L/d$, length L, and diameter d are shown in table 1. Note that batches (II) and (III) have very different lengths and diameters, but roughly the same aspect ratio of $A \approx 6 - 7$.

The rigid fibres were suspended in a Newtonian fluid that had a matching density of $\rho_f = 1056$ kg/m^3. The suspending fluid was a mixture of water (10.72 wt%), Triton X-100 (75.78 wt%), and Zinc Chloride (13.50 wt%). The fluid viscosity of $\eta_f = 3$ Pa·s and the density were measured at the same temperature (25°C) at which the experiments were performed. The suspensions were prepared by adding the fibres to the fluid, where both quantities were weighed, and gently stirring. Little to no settling or creaming was observed.

The rheological measurements were performed at a maximum shear rate of $\dot{\gamma} \approx 3$ s^{-1}, ensuring that a maximum Reynolds number ($\rho_f \dot{\gamma} L^2/\mu_f$) of 0.04 was achieved. The fibres can be considered non-colloidal, owing to their large size, and rigid under the conditions of the experiment. Regarding the latter, the buckling criterion has been characterised by

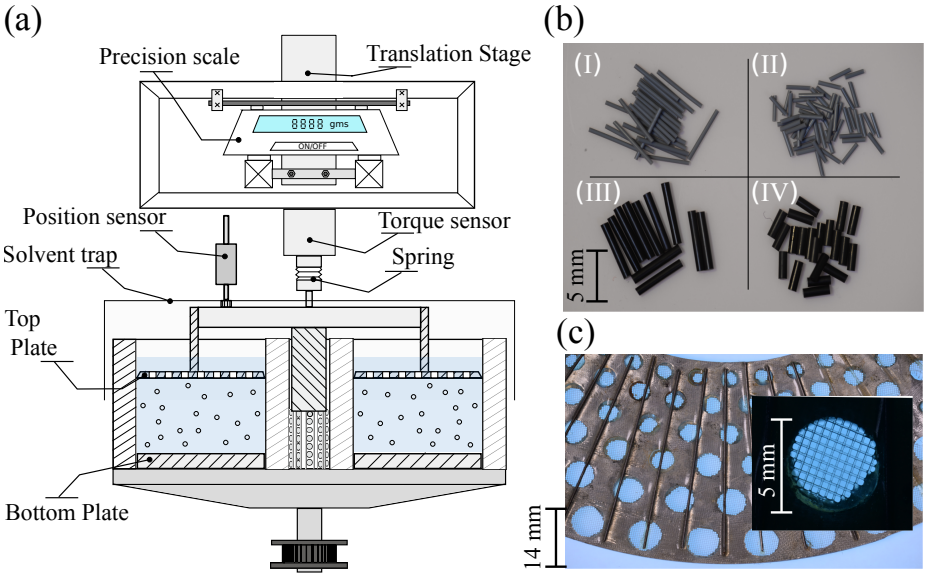

Figure 1: (a) Sketch of the experimental apparatus. (b) Images of the plastic fibres. (c) Image of the top plate (the inset is a blowup of the image showing the nylon mesh).

a dimensionless number, $S_p = 128\,\eta_f \dot{\gamma}\, A^4/E_Y \ln(2A)$, where the Young's modulus, E_Y, is approximately 3000 MPa for PLASTINYL 6.6. The number S_p, often called the Sperm number, is a ratio of the viscous and elastic forces acting on the fibre (see e.g. Becker & Shelley 2001). The values of S_p, shown in table 1 for our experiments, were much smaller than the critical Sperm number of 328 for the coil-stretch transition in a cellular flow (Young & Shelley 2007).

2.2. *Experimental techniques*

The experiments were conducted using a custom rheometer that was originally constructed by Boyer *et al.* (2011) and then modified by Dagois-Bohy *et al.* (2015). This rheometer, sketched in figure 1 (a), provides measurements of both shear and normal stresses. The shearing cell consists of (i) an annular cylinder (of radii $R_1 = 43.95$ mm and $R_2 = 90.28$ mm) which is attached to a bottom plate that can be rotated and (ii) a top cover plate that can be moved vertically. This top plate is porous, enabling fluid to flow through it, but not particles. The plate was manufactured with holes of sizes $2 - 5$ mm and then was covered by a 0.2 mm nylon mesh (see figure 1 (c)). The parallel bottom and top plates have also been roughened by positioning regularly-spaced strips of height and width 0.5 mm onto their surfaces. A transparent solvent trap covers the cell, hindering evaporation of the suspending fluid.

In a typical experiment, the annular cell was filled with suspension and the porous plate was lowered into the fluid to a position h. This height, measured independently by a position sensor (Novotechnik T-50), ranges between 10.8 to 18 mm, corresponding to 13 to 25 fibre diameters depending on the fibre batch. The height measurement enables calculation of the fibre volume fraction, ϕ. The bottom annulus was rotated at a rate Ω by an asynchronous motor (Parvalux SD18) regulated by a frequency controller (OMRON MX2 0.4 kW), while the torque exerted on the top plate was measured by a torque transducer (TEI – CFF401). The shear stress τ was deduced from these torque

measurements after calibration with a pure fluid to subtract undesired contributions resulting from the friction at the central axis and the shear in the thin gap between the top plate and the cell walls; the calibration method is decribed by Dagois-Bohy *et al.* (2015). A precision scale (Mettler-Toledo XS6002S) was placed on a vertical translation stage driven by a LabVIEW code in order to measure the apparent weight of the top plate. This measurements, after correcting for buoyancy, provided the determination of the normal force that the particles exert on the porous plate in the gradient direction. Dividing by the area of the plate gives the gradient component of the normal stress, which is referred to simply as the particle pressure, P. A normal viscosity in the gradient direction can be defined as $P/\eta_f\dot{\gamma}$, as was done by Morris & Boulay (1999).

The rheometer can be run in a pressure-imposed mode or in a volume-imposed mode, and measurements were recorded as a function of the mean shear rate, $\dot{\gamma} = \Omega(R_2 + R_1)/2h$, once steady state was achieved. In pressure-imposed rheometry, the particle pressure P is maintained at a set value that is measured by the precision scale; the volume fraction ϕ and the shear stress τ are measured as a function of the shear rate $\dot{\gamma}$ and pressure P. In volume-imposed rheometry, the height h, and consequently the volume fraction ϕ, are maintained at a fixed value, while the shear stress, τ, and particle pressure, P, are measured as a function of the shear rate, $\dot{\gamma}$. Errors in the measurements of τ, P, and ϕ for the suspensions depend upon the calibration experiments, the preparation of the suspension samples, and the precision of the height, torque, and scale measurements. Estimates, based upon tests with independently created samples of suspension, suggest errors of ± 6 Pa, ± 5 Pa, and ± 0.005 for τ, P, and ϕ, respectively.

3. Rheological measurements

3.1. *Rheological observations*

Typical rheological data for the apparent relative shear and normal viscosities, $\tau/\eta_f\dot{\gamma}$ and $P/\eta_f\dot{\gamma}$, are plotted against volume fraction, ϕ, in figures 2 (a) and (b). The data was collected for fibres of batch (II) using pressure-imposed and volume-imposed measurements. As expected, both quantities increase with increasing ϕ. However, multiple values of the apparent viscosities are measured for any given ϕ. Plotting the shear stress, τ, and the particle pressure, P, against the shear rate for different values of ϕ demonstrates that τ and P are linear in $\dot{\gamma}$, but have a non-zero value at $\dot{\gamma} = 0$, see figures 3 (a) and (b). This seems to suggest that a yield-stress exists for both the shear stress and the particle pressure, τ_0 and P_0, respectively. Their values can be determined using a linear fit of the stress and pressure data as a function of $\dot{\gamma}$, as indicated by the lines in figures 3 (a) and (b). Both yield-stresses, τ_0 and P_0, increase with increasing ϕ as shown in figures 3 (c) and (d) for all four batches of fibres. The growth in τ_0 and P_0 with respect to ϕ is more pronounced for larger aspect ratios A.

The data of figures 3 (a) and (b) demonstrate that the stresses scale linearly with the rate of shear, as expected. Furthermore, the slopes of τ and P with $\dot{\gamma}$ increase with ϕ, which is evidence of the increase of the shear and normal viscosities with ϕ. These shear and normal viscosities can be collapsed into a single function of ϕ by removing the yield stresses. Figures 2 (c) and (d) show the results of $(\tau - \tau_0)/\eta_f\dot{\gamma}$ and $(P - P_0)/\eta_f\dot{\gamma}$ as a function of ϕ. In all of the following analysis, the yield stresses are subtracted systematically from the raw data.

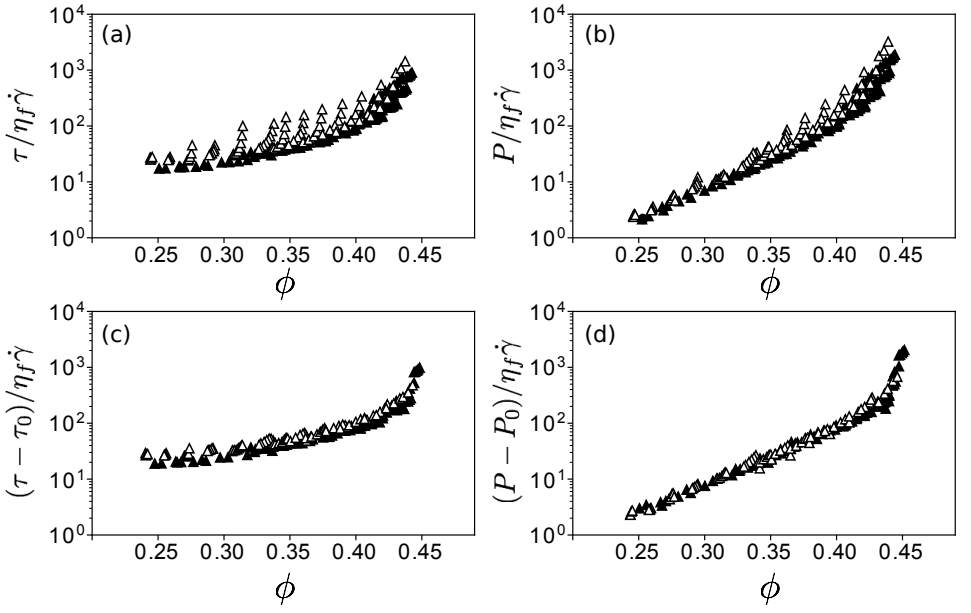

Figure 2: Apparent relative (a) shear ($\tau/\eta_f\dot{\gamma}$) and (b) normal ($P/\eta_f\dot{\gamma}$) viscosities as well as relative (c) shear [$(\tau-\tau_0)/\eta_f\dot{\gamma}$] and (d) normal [$(P-P_0)/\eta_f\dot{\gamma}$] viscosities (after subtraction of the yield-stresses) versus volume fraction, ϕ, for the fibres of batch (II) in pressure-imposed (▲) and volume-imposed (△) configurations.

3.2. *Constitutive laws*

Figures 4 (a) and (b) show $\eta_s = (\tau-\tau_0)/\eta_f\dot{\gamma}$ and $\eta_n = (P-P_0)/\eta_f\dot{\gamma}$, the relative shear viscosity and relative normal viscosity, for all of the fibre batches. Both quantities increase with ϕ and seem to diverge at a maximum volume fraction that depends on the aspect ratio A. The influence of the aspect ratio is also seen on the rheological functions as $\eta_s(\phi)$ and $\eta_n(\phi)$ shift toward lower values of ϕ with increasing A. An interesting observation is that the data for batches (II) and (III), corresponding to similar values of A but different sizes, collapse onto the same curve. This indicates that finite size effects are not significant. Also, the decrease of η_n is much stronger than that of η_s for $\phi \lesssim 0.35$.

An alternative representation of the rheological data plots the friction coefficient $\mu = \eta_s/\eta_n$ and the volume fraction ϕ as a function of the dimensionless shear rate, $J = \eta_f\dot{\gamma}/(P-P_0)$ (Boyer *et al.* 2011); note that $J = 1/\eta_n$ and is a function of ϕ as shown in figure 4b. The rheology is then described by the two functions $\mu(J)$ and $\phi(J)$ as shown in figures 4 (c) and (d) for the same data as in figures 4 (a) and (b). A striking result is that a complete collapse of all the data is observed for $\mu(J)$, indicating that the friction coefficient is independent of the aspect ratio A. The volume fraction ϕ is a decreasing function of the dimensionless number J. There is a clear shift of $\phi(J)$ toward the lower values of ϕ when A is increased. The data for batches (II) and (III), having similar aspect ratios, again collapse onto the same curve.

This frictional approach is particularly well suited to study the jamming transition, as it circumvents the divergence of the viscosities. From the semi-logarithmic plot of $\phi(J)$, shown in the inset of figure 4 (d), the critical (or maximum flowable) volume fraction ϕ_m can be determined from the limiting value of ϕ as J goes to zero. Similarly, the

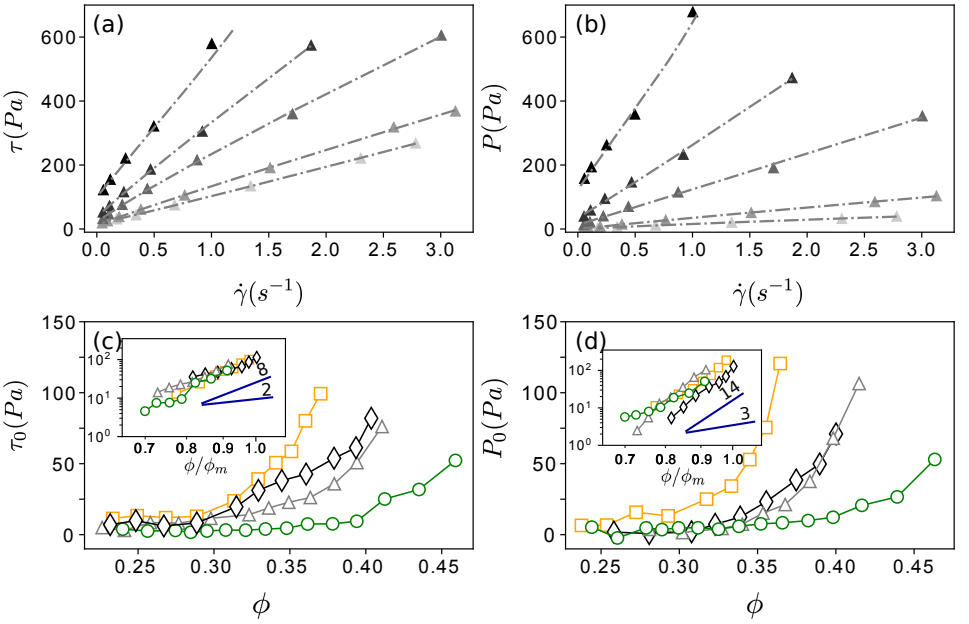

Figure 3: (a) Shear stress (τ) and (b) particle pressure (P) versus shear rate, $\dot{\gamma}$, for the fibre suspension of batch (II) at different ϕ values of 0.26 (lightest grey shade), 0.30, 0.35, 0.38, and 0.41 (black). The lines represent the linear fit for each different ϕ value. Yield-stress (c) for the shear stress (τ_0) and (d) particle pressure (P_0) versus ϕ for fibres of batch (I), (II), (III), and (IV) shown using the symbols □, △, ◊, and ◯, respectively (see table 1). The insets of graphs (c) and (d) are log-log plots versus ϕ/ϕ_m where ϕ_m is the maximum flowable volume fraction given in figure 5 (a).

semilogarithmic plot of $\mu(J)$ in the inset of figure 4 (c) shows that the friction coefficient tends to a finite value μ_s at the jamming point.

The critical values ϕ_m and μ_s are plotted against the fibre aspect ratio A in figures 5 (a) and (b), respectively. Again, the similar results for batches (II) and (III) indicate that confinement is not influencing the measurements, and the values obtained by Boyer *et al.* (2011) for suspensions of poly(methyl methacrylate) spheres are also plotted on these graphs (for $A = 1$, although strictly speaking a sphere is not a cylinder of aspect ratio one). Clearly, ϕ_m decreases with increasing A. This follows the general trends of a decrease in volume fraction with the aspect ratio for processes such as dry packing, as shown in figure 5 (a). A comparison is also made in figure 5 (a) between the values of ϕ_m and estimates from simulations (Williams & Philipse 2003) of the maximum concentration at which the orientation distribution remains random. The critical friction μ_s does not vary significantly with A in the explored range and its value (≈ 0.47) is larger than that obtained for spheres (≈ 0.32) by Boyer *et al.* (2011).

Figure 6 displays the same data as figure 4, but with ϕ scaled by ϕ_m. This simple rescaling leads to a good collapse of the data for all of the fibre batches, indicating that the aspect ratio principally impacts the maximum volume fraction, ϕ_m. Another remarkable result is that the relative shear and normal viscosities, η_s and η_n, diverge near the jamming transition with a scaling close to $(\phi_m - \phi)^{-1}$, as clearly evidenced by the insets of figures 6 (a) and (b). This starkly contrasts with the divergence of $(\phi_m - \phi)^{-2}$ observed for suspensions of spheres (Boyer *et al.* 2011).

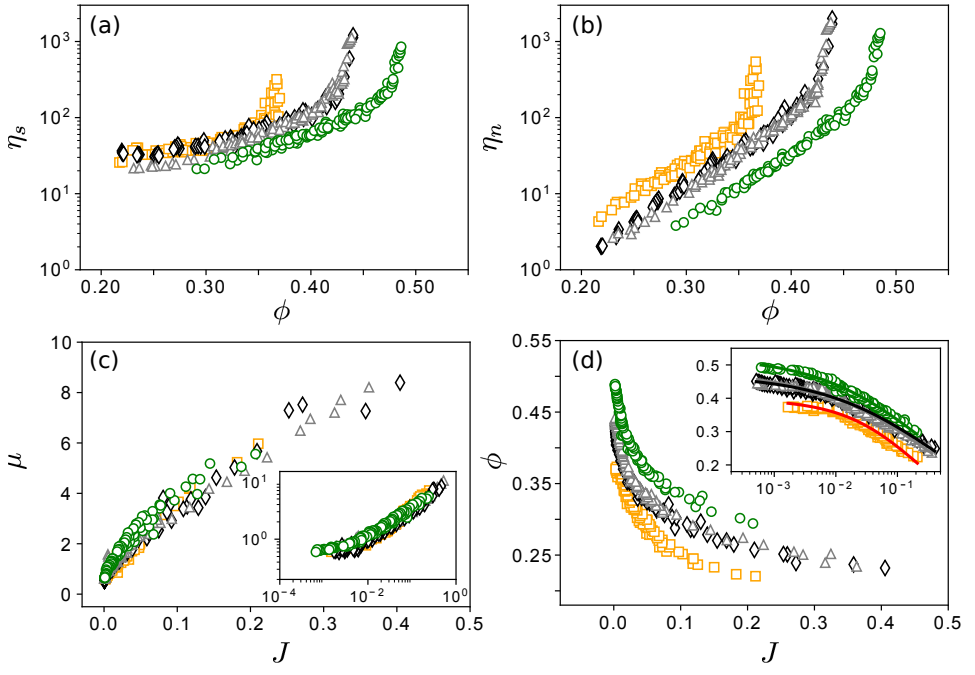

Figure 4: Rheological data: (a) $\eta_s = (\tau - \tau_0)/\eta_f\dot{\gamma}$ and (b) $\eta_n = (P - P_0)/\eta_f\dot{\gamma}$ versus ϕ as well as (c) $\mu = \eta_s/\eta_n$ and (d) ϕ versus $J = \eta_f\dot{\gamma}/(P - P_0)$, for fibre batches (I), (II), (III), and (IV) as represented by the symbols □, △, ◊, and ◯, respectively (see table 1). The insets of graphs (c) and (d) are log-log and semi-logarithmic plots.

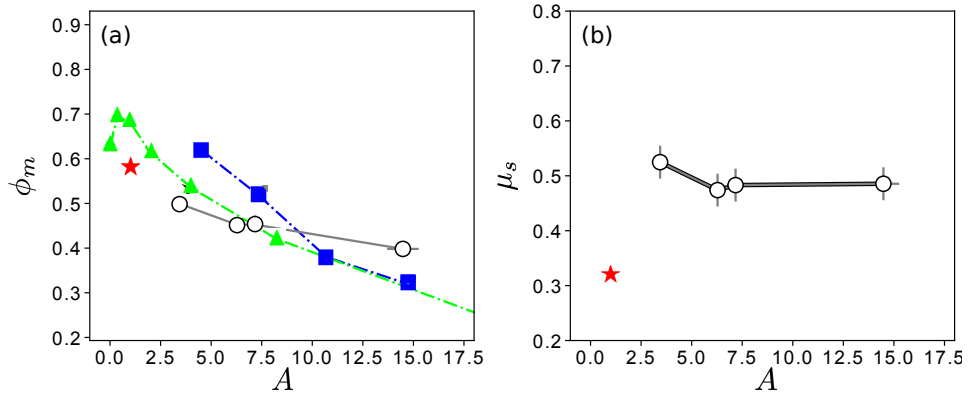

Figure 5: Critical values (a) ϕ_m (◯) and (b) μ_s (◯) at the jamming point versus fibre aspect ratio, A, together with the data (★) obtained by Boyer *et al.* (2011) for suspensions of spheres ($A = 1$). Estimated errors in the values of ϕ_m are smaller than the symbols. Comparisons with experimental data from Rahli *et al.* (1999) (■) on the dry packing of rigid fibres and the simulations of Williams & Philipse (2003) (▲) for the maximum random packing of spherocylinders are given on graph (a).

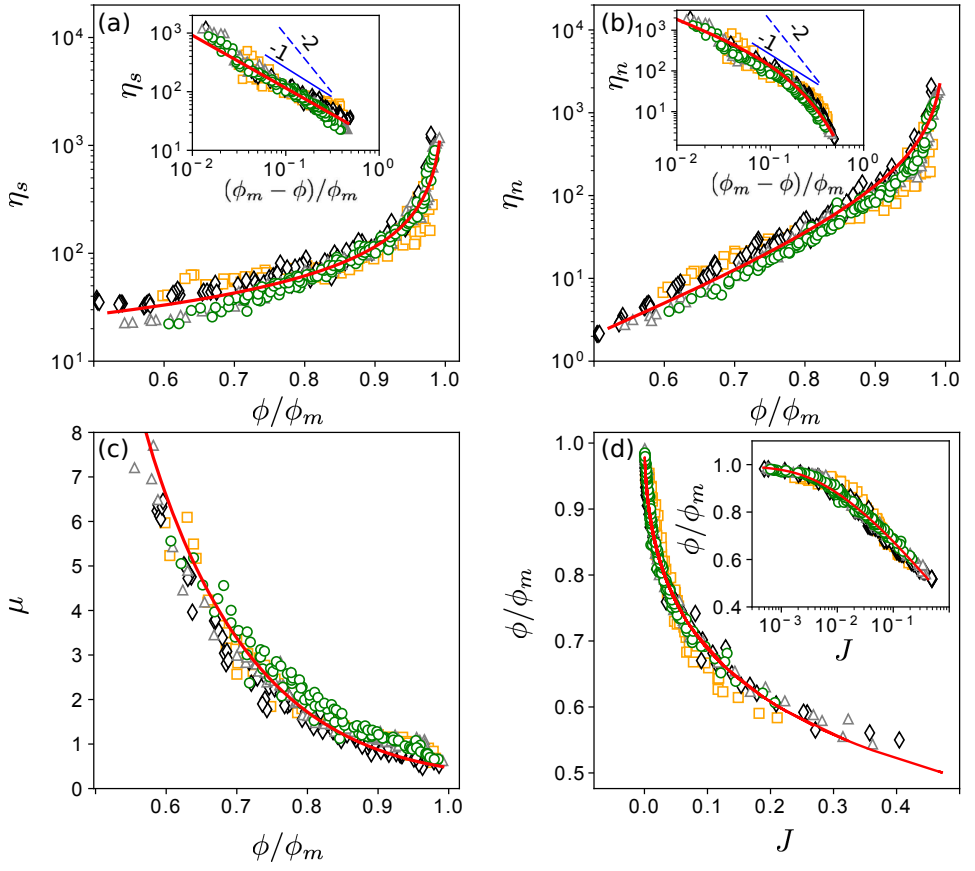

Figure 6: Rescaled rheological data: (a) $\eta_s = (\tau - \tau_0)/\eta_f\dot{\gamma}$, (b) $\eta_n = (P - P_0)/\eta_f\dot{\gamma}$ and (c) $\mu = \eta_s/\eta_n$ versus ϕ/ϕ_m as well as (d) ϕ/ϕ_m versus $J = \eta_f\dot{\gamma}/(P - P_0)$, for all the data of the different batches (I), (II), (III), and (IV) shown using the symbols □, △, ◊, and ◯, respectively (see table 1). The insets of graphs (a), (b), and (d) are log-log plots. The red solid curves correspond to the rheological laws given by equations (3.1), (3.2), and (3.3).

A constitutive law for μ can be generated by fitting the data to a linear combination of powers of $(\phi_m - \phi)/\phi$,

$$\mu(\phi) = \mu_s + \alpha\left(\frac{\phi_m - \phi}{\phi}\right) + \beta\left(\frac{\phi_m - \phi}{\phi}\right)^2, \tag{3.1}$$

as was done by Dagois-Bohy *et al.* (2015). The red curve in figure 6 (c) shows the result, with $\mu_s = 0.47$, $\alpha = 2.44$, and $\beta = 10.20$. As noted previously, the value for μ_s is larger than that obtained for suspensions of spheres ($\mu_s = 0.3$). The values for α and β also differ from those obtained for suspensions of spheres ($\alpha = 4.6$ and $\beta = 6$). The best fit for η_s was found to be

$$\eta_s(\phi) = 14.51\left(\frac{\phi_m - \phi}{\phi_m}\right)^{-0.90}, \tag{3.2}$$

as seen in figure 6 (a). Note that the best-fit exponent is -0.9, rather than -1. The

rheological law for η_n is then just given by

$$\eta_n(\phi) = \eta_s(\phi)/\mu(\phi), \tag{3.3}$$

which is represented by the red curve in figure 6 (b). The variation of ϕ with J can be deduced from this last law since $J = 1/\eta_n(\phi)$; this result is shown in figure 6 (d).

4. Discussion and Conclusions

Using a custom rheometer (Boyer *et al.* 2011; Dagois-Bohy *et al.* 2015), we have performed pressure and volume-imposed measurements of the rheology of non-colloidal rigid fibres suspended in a Newtonian fluid. Measurements for the shear stress and particle pressure have been obtained in the dense regime and for aspect ratios between 3 and 15, and the volume fractions at which the rheology diverges has been characterised as a function of the aspect ratio.

The suspensions exhibit yield-stresses which increase with increasing volume fraction, ϕ, and are more pronounced for larger aspect ratios. Yield-stresses have been reported previously for rigid fibres suspended in Newtonian fluids, and the yield stresses have been attributed to adhesive contacts (see e.g. Mongruel & Cloitre 1999; Chaouche & Koch 2001) despite the relatively large size of the fibres. A recent model (Bounoua *et al.* 2016*b*), which considered attractive interactions between fibres in the dilute regime, predicted simple Bingham laws for both the shear stress and the first normal stress difference, with the apparent shear and normal yield stresses proportional to ϕ^2 and ϕ^3, respectively. The present data also follows Bingham laws, but the yield stress, τ_0, and pressure, P_0, increase with higher power laws in ϕ than predicted. This can be seen in the insets of figures 3 (c) and (d), where it is also demonstrated that the data for all aspect ratios collapses onto single curves by rescaling ϕ by ϕ_m.

It is unclear whether, for the large fibres used here, colloidal forces are responsible for the yield-stresses. Finite-size effects close to the jamming point can also be advocated, particularly since lubrication forces are inefficient at preventing mechanical contacts between elongated particles (Sundararajakumar & Koch 1997). Close to jamming, since the system has a finite size, percolating jamming network of particles can exist. While it is transient phenomenon, it may impact the averaged rheological measurements which consequently may exhibit apparent yield stresses. Clearly, more work is necessary to elucidate the origin of the yield stresses.

Subtracting the apparent yield-stresses reveals a viscous scaling for both the shear stresses and particle pressures, wherein both grow linearly with the rate of shear. The aspect ratio of the fibres does not affect the friction coefficient, μ, but does impact the maximum flowable volume fraction, ϕ_m. Rescaling the volume fraction, ϕ, by this maximum volume fraction, ϕ_m, leads to an excellent collapse of all the data on master curves for the shear and normal viscosities. Hence, we argue that the aspect ratio principally affects the maximum volume fraction at which the suspensions can be sheared. Similar collapse of the rheological data across multiple aspect ratios has been observed previously for shear-thickening suspensions of colloidal fibres (Brown *et al.* 2011).

Using the data presented here, constitutive laws in the form of expansions in $(\phi_m - \phi)$ have been generated for the rheology of dense suspensions of rigid fibres. An important product of the present study is the examination of the rheology close to the jamming transition. At jamming the friction coefficient is found to be constant and to be larger than that found for suspensions of spheres. Both shear and normal viscosities present a similar algebraic divergence in $\approx (\phi_m - \phi)^{-1}$ in stark contrast to that in $(\phi_m - \phi)^{-2}$ observed for suspensions of spheres near the jamming point. The maximum volume

fraction ϕ_m is seen to decrease with increasing aspect ratio, similar to the dry packing of rigid fibres found in experiments (Rahli *et al.* 1999), see figure 5 (a). However, no inferences about the general structure of the suspension at jamming is possible for $A < 15$, as comparisons with estimates of maximum random packing (Williams & Philipse 2003) do not clearly indicate that the orientation distribution has organised. The comparsion does indicate that the structure is organised for $A = 15$, though direct observations, or simulations, of the structures need to be developed in future work to conclusively resolve this question. The experimental data are available as supplementary material for future comparison.

Acknowledgments

We thank Simone Dagois-Bohy for his generous assistance with the experiments. This work is undertaken under the auspices of the ANR project 'Dense Particulate Systems' (ANR-13-IS09-0005-01), the 'Laboratoire d'Excellence Mécanique et Complexité' (ANR-11-LABX-0092), and the Excellence Initiative of Aix-Marseille University - A*MIDEX, a French "Investissements d'Avenir programme", and COST Action MP1305 'Flowing Matter'. FT benefited from a fellowship of CONICYT and SS from a fellowship of the A*MIDEX Excellence Academy - PhD Collegium. The plastic filaments were donated by PLASTICFIBRE S.P.A. This work was also supported by the National Science Foundation (grants #1511787 and #1362060).

REFERENCES

Becker, L. E. & Shelley, M. J. 2001 Instability of elastic filaments in shear flow yields first normal stress differences. *Phys. Rev. Lett.* **87** (19), 198301.

Bibbó, M. A. 1987 Rheology of semiconcentrated fiber suspensions. PhD thesis, Massachusetts Institute of Technology.

Bounoua, S., Lemaire, É., Férec, J., Ausias, G. & Kuzhir, P. 2016*a* Shear-thinning in concentrated rigid fiber suspensions: Aggregation induced by adhesive interactions. *J. Rheol* **60** (6), 1279–1300.

Bounoua, S., Lemaire, É., Férec, J., Ausias, G., Zubarev, A. & Kuzhir, P. 2016*b* Apparent yield stress in rigid fibre suspensions: the role of attractive colloidal interactions. *J. Fluid Mech.* **802**, 611–633.

Boyer, F., Guazzelli, É. & Pouliquen, O. 2011 Unifying suspension and granular rheology. *Phys. Rev. Lett.* **107** (18), 188301.

Brown, E., Zhang, H., Forman, N. A., Maynor, B. W., Betts, D. E., DeSimone, J. M. & Jaeger, H. M. 2011 Shear thickening and jamming in densely packed suspensions of different particle shapes. *Phys. Rev. E* **84** (3), 031408.

Chaouche, M. & Koch, D. L. 2001 Rheology of non-Brownian rigid fiber suspensions with adhesive contacts. *J. Rheol.* **45** (2), 369–382.

Dagois-Bohy, S., Hormozi, S., Guazzelli, É. & Pouliquen, O. 2015 Rheology of dense suspensions of non-colloidal spheres in yield-stress fluids. *J. Fluid Mech.* **776**, R2.

Dinh, S. M. & Armstrong, R. C. 1984 A rheological equation of state for semiconcentrated fiber suspensions. *J. Rheol.* **28**, 207–227.

Egres, R. G. & Wagner, N. J. 2005 The rheology and microstructure of acicular precipitated calcium carbonate colloidal suspensions through the shear thickening transition. *J. Rheol.* **49** (3), 719–746.

Ganani, E. & Powell, R. L. 1985 Suspensions of rodlike particles: Literature review and data correlations. *J. Comp. Mat.* **19**, 194–215.

Mongruel, A. & Cloitre, M. 1999 Shear viscosity of suspensions of aligned non-Brownian fibres. *Rheol. Acta* **38** (5), 451–457.

Morris, J. F. & Boulay, F. 1999 Curvilinear flows of noncolloidal suspensions: The role of normal stresses. *J. Rheol.* **43** (5), 1213–1237.

Petrich, M. P. & Koch, D. L. 1998 Interactions between contacting fibers. *Phys. Fluids* **10** (8), 2111–2113.

Powell, R.L. 1991 Rheology of suspensions of rodlike particles. *J. Stat. Phys.* **62**.

Rahli, O., Tadrist, L. & Blanc, R. 1999 Experimental analysis of the porosity of randomly packed rigid fibers. *C. R. Acad. Sci., Ser. IIb: Mec., Phys., Chim., Astron.* **327** (8), 725–729.

Sepehr, M., Carreau, P. J., Moan, M. & Ausias, G. 2004 Rheological properties of short fiber model suspensions. *J. Rheol.* **48**, 1023–1048.

Snook, B., Davidson, L. M., Butler, J. E., Pouliquen, O. & Guazzelli, É. 2014 Normal stress differences in suspensions of rigid fibres. *J. Fluid Mech.* **758**, 486–507.

Sundararajakumar, R. & Koch, D. L. 1997 Structure and properties of sheared fiber suspensions with mechanical contacts. *J. Non-Newtonian Fluid Mech.* **73**, 205–239.

Williams, S. R. & Philipse, A. P. 2003 Random packings of spheres and spherocylinders simulated by mechanical contraction. *Phys. Rev. E* **67** (5), 051301–9.

Young, Y. N. & Shelley, M. J. 2007 Stretch-coil transition and transport of fibers in cellular flows. *Phys. Rev. Lett.* **99** (5), 58303.